Journal of Building Engineering 116 (2025) 114605

Contents lists available at ScienceDirect

Journal of Building Engineering

journal homepage: www.elsevier.com/locate/jobe

Cyclic seismic in-plane performance of precast lightweight aggregate concrete insulation panels with splice-sleeve-based bolting technique

Keun-Hyeok Yang [a], Ju-Hyun Mun [a,*], Jong-Won Kim [a], Hye-Ji Lee [b]

[a] Department of Architectural Engineering, Kyonggi University, Suwon, Kyonggi–do, Republic of Korea
[b] Department of Architectural Engineering, Kyonggi University, Graduate School, Suwon, Kyonggi–do, Republic of Korea

ARTICLE INFO

Keywords:
Precast lightweight aggregate concrete panels
Cyclic seismic in-plane performance
Panel-to-base connection
Splice-sleeve-based bolting technique

ABSTRACT

This study investigated the cyclic seismic in-plane performance of meta-based insulated precast lightweight aggregate concrete panels (HMI-panels) using a novel splice-sleeve-based bolting technique. The primary objective was to evaluate the structural safety and seismic behavior of this innovative connection method, focusing on key design parameters such as vertical reinforcement ratios and base-to-panel connection types. Four specimens were prepared and subjected to cyclic lateral loading tests to analyze the crack propagation, failure modes, load–displacement relationships, cracking and maximum flexural moments, displacement ductility ratios, and cumulative dissipated energies. The test results were compared with predictions based on the ACI 318-19 standards and one-dimensional nonlinear analysis procedures to validate the structural safety of the proposed splice-sleeve-based bolting technique. The findings demonstrate that the splice-sleeve-based bolting technique provides superior lateral load resistance and ductility compared to conventional methods such as L-shaped steel-plate-based bolting. Specimens connected using this technique exhibited effective load transfer, minimal slip at the joints, and flexural behavior comparable to that of traditional splice-sleeve systems. Moreover, the enhanced constructability and elimination of on-site grouting processes highlight the practical advantages of precast construction. This study concludes that the proposed splice-sleeve-based bolting technique is a viable solution for improving the seismic performance of HMI-panels while maintaining their structural safety and efficiency.

1. Introduction

Precast concrete panels with internal insulation (PC insulated panels) are gaining popularity as products that can simultaneously achieve thermal insulation and fire resistance, meeting the increasingly stringent requirements for the thermal transmittance of exterior walls and fire safety of insulation materials in buildings [1]. In particular, meta-based panels are attracting increasing attention as exterior cladding systems capable of providing both thermal insulation and fire resistance. In this study, the term meta-based panel is defined as a type of PC-insulated panel in which internal structures or metamaterials are embedded within the concrete to enhance both thermal insulation and fire resistance. Consequently, PC-insulated panels are widely used as exterior

* Corresponding author.
E-mail addresses: yangkh@kgu.ac.kr (K.-H. Yang), mjh@kgu.ac.kr (J.-H. Mun), slaslek@naver.com (J.-W. Kim), gpwldud068@naver.com (H.-J. Lee).

https://doi.org/10.1016/j.jobe.2025.114605
Received 27 March 2025; Received in revised form 4 November 2025; Accepted 8 November 2025
Available online 11 November 2025

claddings, and because of their large size and heavy weight, they require safe connection techniques when attached to building exteriors [2]. Although PC-insulated panels are considered non-structural components that serve as building finishes, they must possess sufficient strength to withstand external forces (wind or seismic loads) to prevent detachment once installed on buildings. Accordingly, recent researchers have continuously performed cyclic lateral load tests to evaluate the seismic performance of such non-structural components [3–9]. These investigations have clarified panel behavior under realistic seismic demands and revealed weaknesses in connection mechanisms. Moreover, the seismic behavior of other non-structural components (including curtain walls, masonry infill panels, and lightweight partition walls) has also been recognized as critical for the overall performance of building envelopes [3–7]. Damage to these elements during earthquakes may cause loss of structural function, extensive repair costs, and even risk to life safety, as detailed in several post-earthquake assessment reports [7,8]. To address these issues, researchers have investigated the behavior and failure mechanisms of different panel types under lateral and cyclic loading, and developed guidelines for improving their seismic performance [8–10]. For example, reinforced infill panels and advanced connection systems for curtain walls have demonstrated improved energy dissipation and ductility, but often entail increased construction complexity or cost. For this reason, KDS 41 17 00 [11] stipulates that non-structural elements should also meet certain seismic performance requirements, such as securing resistance to design earthquake loads at joints and relative displacement due to earthquakes. Ensuring seismic performance is essential even for non-structural PC insulated panels, and various connection techniques with enhanced seismic performance are being developed to meet this requirement [12–16]. Deng et al. [4] evaluated the effects of various horizontal connections on the out-of-plane structural performance of a single-face superposed shear wall designed to compensate for the reduction in load resistance caused by insulation. Yang et al. [13] examined the effects of different panel-to-base connection techniques on the out-of-plane flexural behavior of precast lightweight aggregate concrete (PLC) panels with embedded honeycomb cardboard for better structural safety against wind and earthquake loads. O'Hegarty and Kinnane [14] evaluated the shear behaviour according to the type and reinforcement details of the connector in the precast concrete panel and suggested an optimal connector design plan. Elbelbisi et al. [15] evaluated the out-of-plane structural performance of sandwich wall panels composed of multiple layers of concrete and insulating cores and emphasized the importance of the types of shear connectors and connection techniques. However, these techniques have mostly verified the safety of connections in the out-of-plane direction rather than in the in-plane direction, and under static monotonic loads rather than cyclic loads.

Nevertheless, in actual building systems, PC-insulated panels are often subjected to significant in-plane forces, particularly during seismic events or large structural deformations caused by inter-story drift and overall frame movement. These in-plane forces induce shear, tensile, and compressive stresses transmitted through the panel connections, increasing the risk of panel detachment and damage under such conditions. Furthermore, observations from recent earthquakes revealed that most failures of cladding panels originated from insufficient in-plane connection resistance, resulting in partial or total detachment as well as reduced energy dissipation and ductility performance [16–19]. Thus, while out-of-plane forces are primarily governed by panel stiffness and connection support, the seismic safety and structural integrity of the entire building envelope are more directly affected by the in-plane resistance of these panels. For this reason, connection techniques for PC-insulated panels should be evaluated primarily based on their in-plane behavior under realistic loading conditions to prevent damage and large-scale detachment, and to enhance the seismic performance and resilience of the structure. Generally, PC-insulated panels require greater connection resistance in the in-plane direction than in the out-of-plane direction, and they experience cyclic loads rather than monotonic loads during earthquakes. In particular, considering the higher resistance required in the in-plane direction for PC-insulated panels and the lower flexural resistance exhibited under cyclic loads compared to monotonic loads, a re-evaluation of the connection safety demonstrated in previous studies [20–22] is necessary. Therefore, in line with current research trends, it is essential to ensure the structural safety of connection techniques under the most unfavorable loading conditions while minimizing on-site processes.

The objective of this study was to evaluate the structural safety of a newly developed splice-sleeve-based base-to-panel connection technique to ensure the cyclic seismic in-plane performance in honeycomb-meta-based insulated PC panels (HMI-panels). The main parameters selected the distributed vertical reinforcement ratio and type of base-to-panel connection, which are the most critical factors affecting the flexural strength and ductility of PC members in terms of seismic behavior. Four specimens were prepared, and structural tests were conducted with cyclic lateral loading in the in-plane direction. The seismic behavior of the HMI-panels was evaluated using the test results of crack propagation, failure modes, lateral load-displacement relationships, cracking and maximum strength moments, displacement ductility ratios, and cumulative dissipated energy. The measured cracking and maximum flexural moments were compared with the values predicted by ACI 318-19 [23] to verify the structural safety of the developed splice-sleeve-based base-to-panel connection technique against cyclic lateral resistance. In particular, the displacement ductility ratios of the HMI-panels were compared with the values predicted by the one-dimensional nonlinear analysis procedure proposed by Mun et al. [24] to verify the ductility capacity of the splice-sleeve-based base-to-panel connection technique.

2. Novel splice-sleeve-based base-to-panel technique

The primary contribution of this study is the development of a novel splice-sleeve-based base-to-panel connection technique for precast concrete panels, which enables factory-controlled grouting and eliminates the need for on-site wet processes. This splice-sleeve-based bolting method was designed to address the limitations of conventional splice-sleeve techniques, specifically improving on-site constructability and ensuring enhanced quality by managing the grouting process in controlled factory conditions. The research objectives are as follows: (1) to propose and detail this innovative connection system, (2) to experimentally validate its mechanical performance, and (3) to assess its potential advantages in terms of structural reliability compared to existing methods. Additionally, the cyclic in-plane seismic behavior of HMI-panels was investigated to provide essential data for seismic design and

construction. Experimental results were analyzed against existing design codes, such as ACI 318-19 [23], and tailored design guidelines for HMI-panels were established. These findings offer actionable information for the design and construction of HMI-panel-integrated buildings, contributing to the broader adoption of precast concrete construction methods and advancing current construction practices.

Fig. 1 illustrates the details of the splice-sleeve-based base-to-panel connection technique. This connection technique consists of a splice sleeve, a welded coupler, and a steel plate. The manufacturing process of PC panels using these components is as follows: 1) a splice sleeve with an outer diameter of 60 mm was embedded at the base joint location along with vertical and horizontal reinforcement in the PC panel. 2) Concrete is poured into the PC panel and cured. 3) The protruding rebar, located at the same position as the vertical reinforcement of the PC panel, was welded to the top of a 20 mm thick steel plate. A welded coupler was attached to the part of the protruding rebar being welded to prevent any degradation of the mechanical properties of the rebar due to welding. 4) The protruding rebar welded to the steel plate was inserted into the splice sleeve pre-embedded in the PC panel and grouted. 5) After curing, the PC panel was fully fixed to the base on-site through the holes formed in the steel plate using bolts and nuts. This method allows the omission of the on-site grouting process associated with the conventional splice-sleeve technique, enabling the production of high-quality PC panels by managing the grouting process in factories. Moreover, this approach is expected to enhance the load transfer capacity of PC panel joints by eliminating on-site wet processes and simplifying connections with manufactured base joints.

However, several potential limitations remain with the newly developed splice-sleeve-based base-to-panel connection technique. First, the success of factory-controlled grouting depends heavily on consistent quality management throughout all stages of the manufacturing process including grout mixing, curing, or sleeve embedding, as any lapses may adversely affect connection performance. Second, although the method allows the omission of on-site wet work, it requires highly precise alignment between the embedded splice sleeves and protruding reinforcing bars during installation, which can challenge constructability when tolerances are minimal or base conditions are irregular. Third, the use of welded couplers and steel plates raises concerns about welding quality and long-term durability, particularly under cyclic or fatigue loading conditions. Finally, additional fabrication processes such as welding and factory grouting may increase production costs or necessitate specialized equipment and skilled labor, potentially limiting widespread adoption in certain construction environments. Continued technological development and field validation are required to further enhance the reliability and cost-effectiveness of the proposed connection system.

3. Experimental details

3.1. Specimen details

Table 1 and Fig. 2 show the details of the HMI-panel specimens. The main parameters for the HMI-panel were the type of base-to-panel connection and the vertical reinforcement ratio (ρ_v). The types of base-to-panel connections include the L-shaped steel-plate-based bolting technique developed by Mun et al. [24], the conventional splice-sleeve technique, and the splice-sleeve-based bolting technique developed in this study. Based on the details developed by Yang et al. [13], the L-shaped steel-plate-based bolting technique

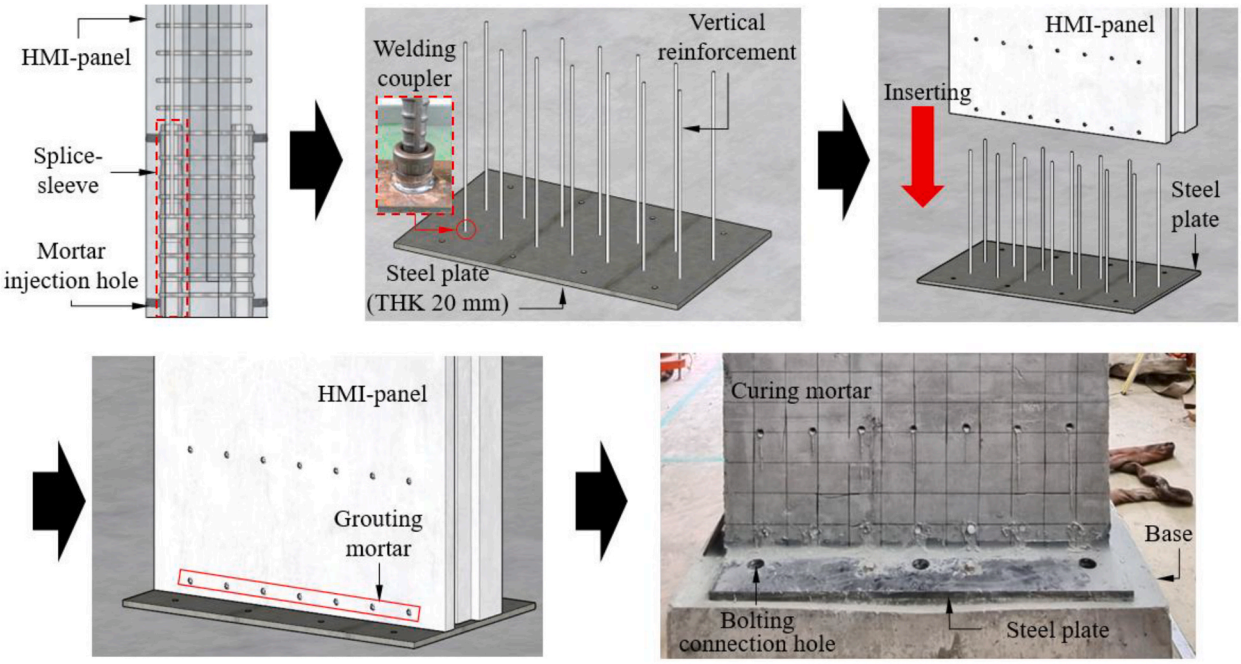

Fig. 1. – Details of splice-sleeve-based base-to-panel connection technique designed to improve constructability and ensure grouting quality.

Table 1
– Details of test specimens according to panel-to-base connection type and longitudinal tensile reinforcement ratio.

Specimens	Main parameters				f_{cd} (MPa)	f_c' (MPa)	w_c (kg/m^3)	V_n (kN) (3)	V_{fl} (kN) (4)	(3)/(4)
	Type of panel-to-base connection	ρ_s (1)	$\rho_{s(\min)}$ (2)	(1)/(2)						
L-1.0	L-shaped steel plate-based bolting technique	0.0029	0.0029	1.0	24	25.4	1468	974	210	4.65
S-1.0	Conventional splice-sleeve technique								214	4.56
W-1.0	Splice-sleeve-based bolting technique								214	4.56
W-1.5		0.0042		1.5					310	3.15

Note: ρ_s = ratio of longitudinal tensile reinforcement, $\rho_{s(\min)}$ = ratio of minimum longitudinal tensile reinforcement determined in accordance with ACI 318-19, f_{cd}' = designed compressive strength of concrete, f_c' = compressive strength of concrete, w_c = unit weight of concrete, V_n = internal shear force, and V_{fl} = internal flexural force.

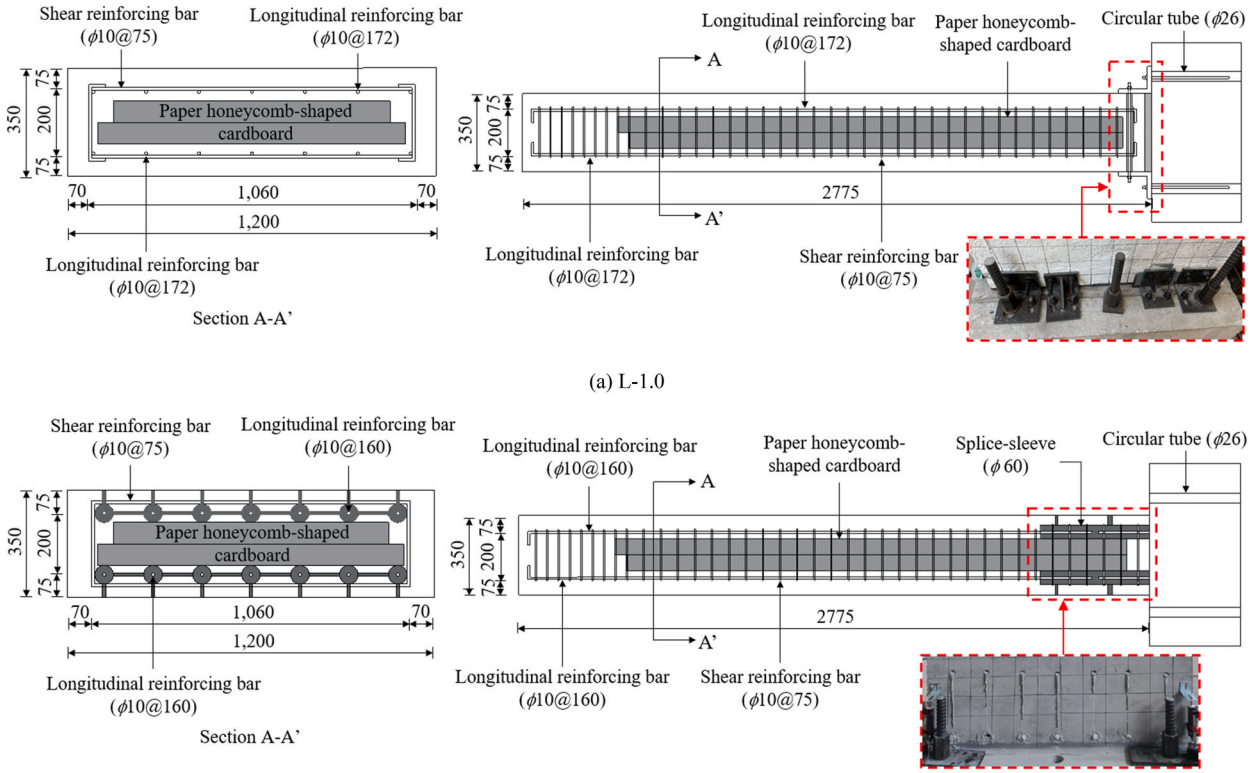

Fig. 2. – Details of HMI-panel specimens according to panel-to-base connection type and longitudinal tensile reinforcement ratio (unit: mm).

connects the base and PC panels using circular steel pipes pre-embedded in the panel, through which threaded bolts and nuts pass (Fig. 2(a)). The conventional splice-sleeve technique connects the base and PC panels by inserting a rebar protruding from the base into the pre-embedded splice sleeves in the panel, followed by a grouting process (Fig. 2(b)). The splice-sleeve-based bolting technique developed in this study is described in detail in Section 2. Additionally, ρ_v was varied to be 1.0 and 1.5 times the minimum vertical reinforcement ratio ($\rho_{v(\min)}$) as suggested by ACI 318-19 [23]. For the HMI-panel specimens with $\rho_v = 1.0\rho_{v(\min)}$, deformed bars with a diameter of 10 mm were vertically reinforced at 160 mm intervals. For specimens with $\rho_v = 1.5\rho_{v(\min)}$, deformed bars with a diameter of 16 mm were vertically reinforced at 320 mm intervals for ease of fabrication.

All the HMI-panel specimens were manufactured with thicknesses (t_w), widths (b_w), and lengths (L) of 350, 1200, and 2775 mm, respectively. The shear reinforcement consisted of deformed bars with a diameter of 10 mm placed at 75 mm intervals, which were determined based on the external shear force (V_{fl}) calculated from the nominal flexural moment (M_n) of the HMI-panel ($V_{fl} < V_n$). To enhance insulation, a double layer of honeycomb metamaterial was placed centrally within each HMI-panel specimen. The thickness,

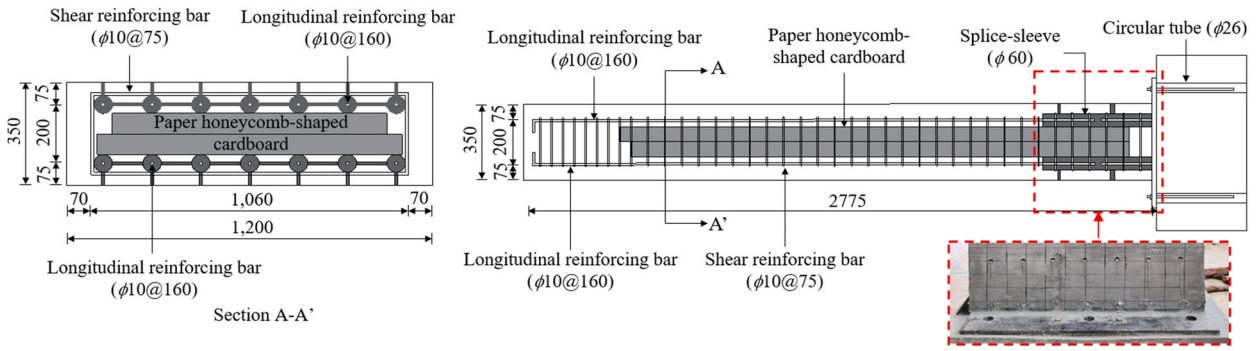

(c) W-1.0

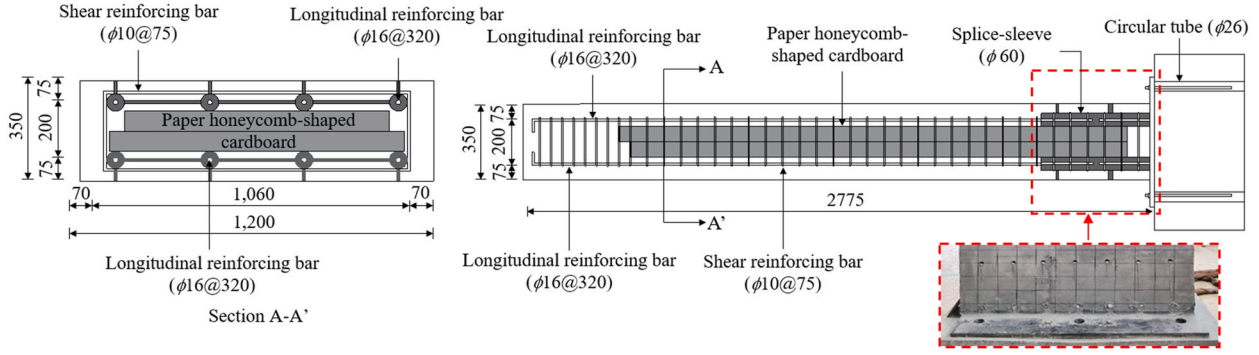

(d) W-1.5

Fig. 2. (*continued*).

width, and length of the inserted honeycomb metamaterial were 70, 1000, and 2250 mm, respectively, based on the findings of Sim et al. [25]. In the specimen names, the letters indicate the connection method with the base (L = L-shaped steel-plate-based bolting technique, S = splice-sleeve technique, SB = splice-sleeve-based bolting technique), and the numbers indicate the ρ_v (1.0 = $1.0\rho_{v(\min)}$, 1.5 = $1.5\rho_{v(\min)}$). For example, S-1.0 refers to an HMI-panel specimen arranged using $\rho_v = 1.0\rho_{v(\min)}$ and connected using the splice-sleeve technique at the base-to-panel joint.

3.2. Material properties

Table 2 presents the mixture proportions of insulating concrete used in the manufacture of the HMI-panels. The mixture proportions were determined based on the experimental results of Kim et al. [26], considering the target compressive strength (f_{cd} = 24 MPa). The determined mixture proportions had a water-binder ratio (W/B) of 30 %, a sand-aggregate ratio (S/a) of 47 %, and a unit binder content of 450 kg/m^3. The cementitious binder consisted of ordinary Portland cement (OPC), ground granulated blast-furnace slag (GGBS), and fly ash (FA) in proportions of 30 %, 50 %, and 20 % of the total binder content, respectively. The densities of OPC, GGBS, and FA were 3.15, 2.94, and 2.2 g/cm^3, respectively, with specific surface areas of 3260, 4355, and 4170 cm^2/g, respectively. To ensure insulation properties, lightweight bottom ash aggregates with low density produced at the Yeong-Heung Thermal Power Plant in Korea were used. To satisfy the particle size distribution requirements of KS F 2527 [27], a combination of lightweight aggregates of various sizes was employed. The fineness modulus of the fine and coarse aggregates was 2.93 and 6.44, respectively. The water

Table 2
– Concrete mixture proportions.

f'_{cd} (MPa)	f'_c (MPa)	W/B (%)	S/a (%)	Unit weight (kg/m^3)								S.P (%)
				W	OPC	GGBS	FA	Fine aggregate		Coarse aggregate		
								2 mm under	2–5 mm	5–10 mm	10–20 mm	
24	25.4	30	47	135	135	225	90	289	123	141	329	0.5

Note: f'_{cd} = designed compressive strength of concrete, f'_c = compressive strength of concrete, W/B = water-to-binder ratio by weight, S/a = fine aggregate-to-total aggregate ratio by volume, W = water, OPC = ordinary Portland cement, GGBS = ground granulated blast-furnace slag, FA = fly ash, and S.P = superplasticizer admixture.

absorption rates were relatively high at 2.71 % for fine aggregates and 6.11 % for coarse aggregates (Table 3). To prevent workability reduction during mixing, these lightweight aggregates were pre-wetted for three days and then used under surface-saturated dry conditions.

The honeycomb meta used a material with a thermal conductivity of 0.1 W/m·K and a density of 0.18 g/cm^3. To prevent concrete's lateral pressure and moisture from penetrating the paper material on the surface where the concrete was poured, a laminate made of synthetic resin was attached. Meanwhile, the yield strength and tensile strength of the reinforcements used were 475 MPa and 608 MPa, respectively, for ϕ10, and 477 MPa and 612 MPa, respectively, for ϕ16. The yield strengths of the threaded bolts and steel pipes were 388 MPa and 485 MPa, respectively, and their tensile strengths were 510 MPa and 612 MPa, respectively. The yield and tensile strengths of the splice sleeves were 558 MPa and 658 MPa, respectively (Table 4).

3.3. Test procedure and instrumentation

Fig. 3 illustrates the test set-up for the HMI-panel specimen. To simulate the cantilever behavior, the lower stub (base) of the HMI-panel specimen was securely fixed to the reaction floor using steel rock bolts and nuts through the penetrated holes. Loading was applied in both the positive and negative directions within the in-plane using a 2000 kN capacity actuator connected to the top of the panel. Fig. 4 shows the loading history of cyclic loads applied to the HMI-panel specimen. The drift ratios at each cycle (0.043 %, 0.055 %, 0.07 %, 0.1 %, 0.14 %, 0.2 %, 0.25 %, 0.33 %, 0.5 %, 0.67 %, and 1 %) were determined following the procedure specified FEMA 356 [28]. The incremental displacements for positive and negative loadings were determined from the drift ratios specified in FEMA 356 [28], with three cycles repeated at each incremental displacement. The incremental displacements of the specimens were measured using a 300 mm capacity linear variable differential transducer (LVDT) installed at the loading point. The slip displacement at the base-to-panel joint was measured using a 50 mm capacity LVDT installed between the top of the lower stub and panel specimen. All of this equipment was provided by the Intelligent Construction System Core Support Center at Keimyung University in Korea. The strain in the reinforcements was measured using electrical resistance strain gauges installed near the base-to-panel joints.

4. Test results and discussion

4.1. Crack propagation and failure mode

Fig. 5 shows the crack propagation and failure modes of the HMI-panel specimens. The crack propagation and failure modes were significantly affected by the base-to-panel connection technique and the vertical reinforcement ratio (ρ_v). For the specimens connected using the L-shaped steel-plate-based bolting technique, cracks were concentrated around the circular steel pipes installed for the base-to-panel connection until the end of the experiment. This was attributed to sliding failure caused by excessive slip in the space between the circular steel pipes and the threaded bolts used for the connection. In contrast, the specimens connected using the conventional splice-sleeve technique and the splice-sleeve-based bolting technique showed different crack propagation patterns. The initial flexural cracks occurred near the base-to-panel connection and gradually progressed upward as the load increased. The height of the upward progression was similar for both techniques but increased slightly with increasing ρ_v values. After the outermost vertical reinforcements yielded, no additional flexural cracks appeared; however, the width of the existing flexural cracks near the base-to-panel connection gradually increased. After reaching the peak load, the outermost vertical reinforcements sequentially fractured until the end of the experiment. Notably, the HMI-panel specimens connected using the conventional splice-sleeve technique and splice-sleeve-based bolting technique showed no observable slip at the connection. Based on these experimental results, it is concluded that the L-shaped steel-plate-based bolting technique does not effectively transfer lateral loads owing to the sliding failure at the base-to-panel connection. In contrast, the conventional splice-sleeve technique and splice-sleeve-based bolting technique are considered to transfer lateral loads effectively, as evidenced by the upward progression of flexural cracks and the fracture pattern of the vertical reinforcements.

Table 3
– Physical properties of bottom ash aggregates.

Aggregate type	Appearance	Maximum size (mm)	Density (g/cm^3)	Fineness modulus	Water absorption (%)
Fine aggregate		5	2.08	2.71	2.93
Coarse aggregate		20	1.84	6.12	6.44

Table 4
– Mechanical properties of the reinforcing steel.

Specimens	Diameter (mm)	Yield strength (MPa)	Yield strain	Tensile strength (MPa)	Elastic modulus (MPa)
Deformed bar	10	475	0.0022	608	218464
	16	477	0.0021	612	223548
Threaded bolt	10	388	0.0020	510	197547
Steel pipe	25	485	0.0025	612	197454
Splice sleeve	60	558	0.0032	658	175881

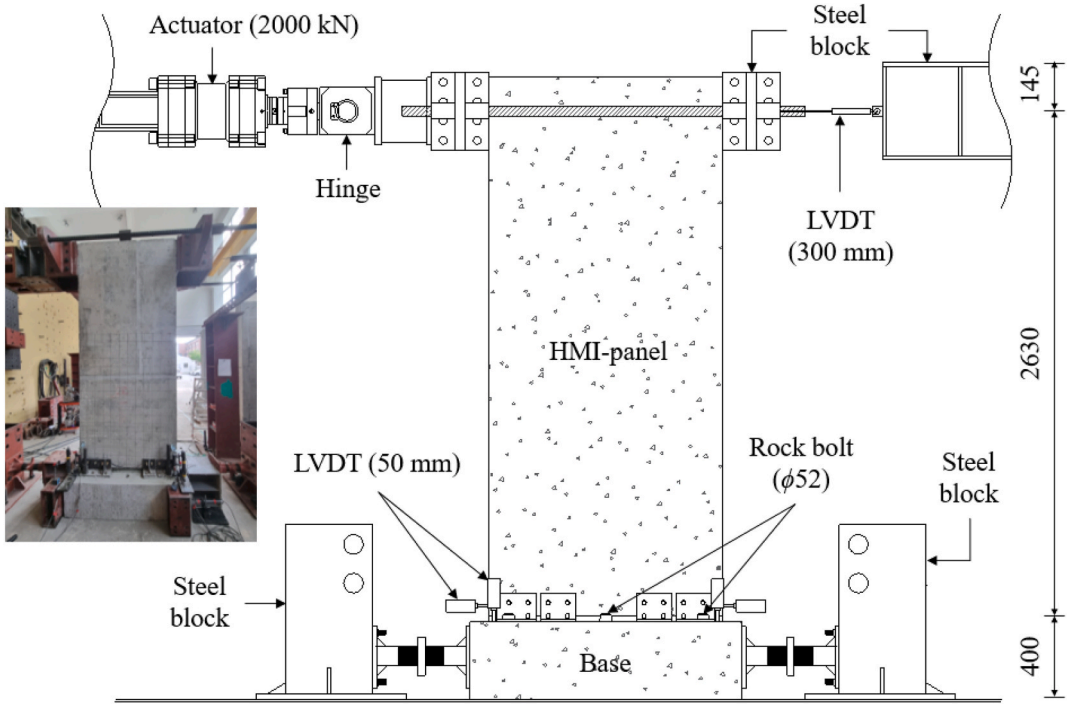

Fig. 3. –Test setup of HMI-panel specimens under cyclic in-plane loading (unit: mm).

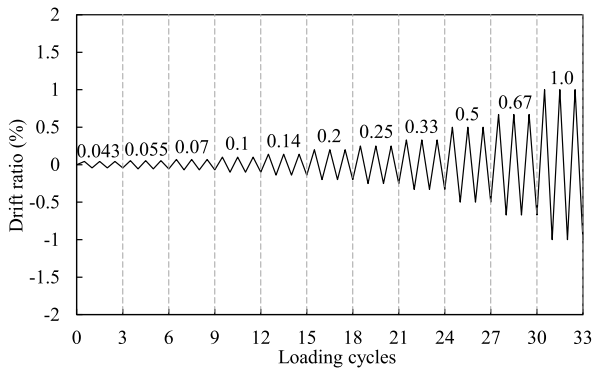

Fig. 4. – Loading history of cyclic loads applied to the HMI-panel specimens.

4.2. Lateral load–displacement relationship

Fig. 6 shows the lateral load–displacement relationships of the HMI-panel specimens. For the specimens connected using the L-shaped steel-plate-based bolting technique, the initial stiffness sharply decreased from the point where the slip occurred at the base-to-panel connection. The lateral load–displacement relationship of this specimen exhibited a typical sliding behavior, where the displacement increased under low loads. In contrast, the specimens connected using the conventional splice-sleeve technique and the

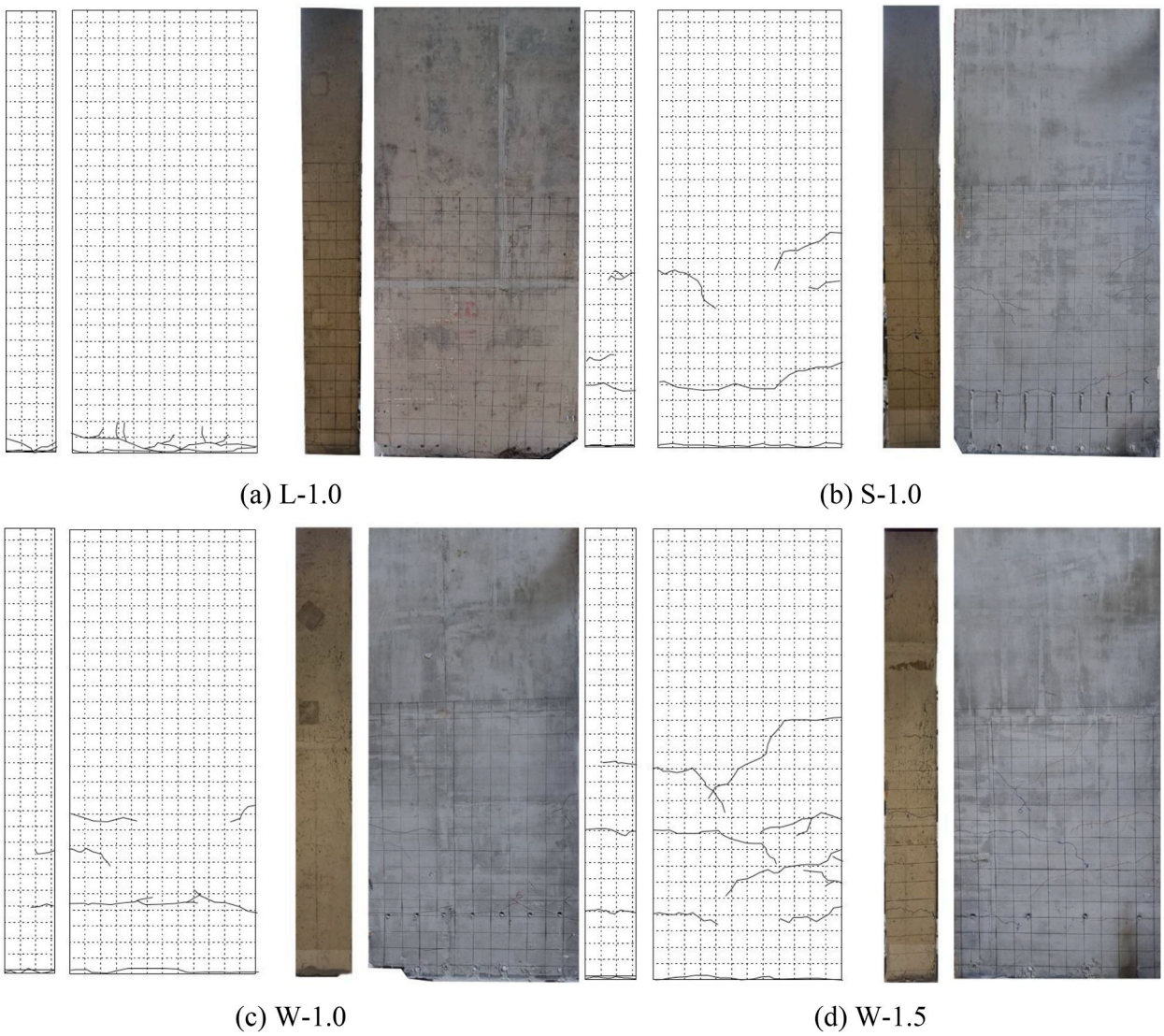

Fig. 5. – Crack propagation and failure mode of HMI-panel specimens under cyclic in-plane loading.

splice-sleeve-based bolting technique maintained linear stiffness up to the yield point, after which the stiffness gradually decreased until the peak load was reached. After reaching the peak load, these specimens displayed a brittle tendency with a rapid decrease in the applied load. Overall, the area of each hysteresis loop in the lateral load–displacement relationship was larger for the conventional splice-sleeve technique and splice-sleeve-based bolting techniques than that for the L-shaped steel-plate-based bolting technique. The largest area was observed for the HMI-panel specimen with the highest vertical reinforcement ratio ($\rho_v = 1.5\rho_{v(\min)}$). Consequently, it was concluded that the splice-sleeve-based bolting technique exhibited flexural behavior comparable to that of the conventional splice-sleeve technique.

4.3. Cracking (P_{cr}) and peak (P_n) loads

Table 5 summarizes the experimental results of the HMI-panel specimens. The cracking load (P_{cr}) of the specimens connected using the L-shaped steel-plate-based bolting technique was 15.4 kN, which is relatively low. In contrast, the P_{cr} values of the specimens connected using the conventional splice-sleeve technique and the splice-sleeve-based bolting technique were 48.4 kN and 49.2 kN, respectively, showing similar levels. These values were approximately 3.17 times higher than those of the specimens connected using the L-shaped steel-plate-based bolting technique. Notably, the P_{cr} value of the specimen connected using the splice-sleeve-based bolting technique was approximately 1.38 times higher when designed with $\rho_v = 1.5\rho_{v(\min)}$ than when designed with $\rho_v = 1.0\rho_{v(\min)}$.

The trend in the peak load (P_n) of the HMI-panel specimens was consistent. The P_n value for the specimen connected using the L-shaped steel-plate-based bolting technique was 36.9 kN, which was the lowest among all specimens. In contrast, the P_n values of the

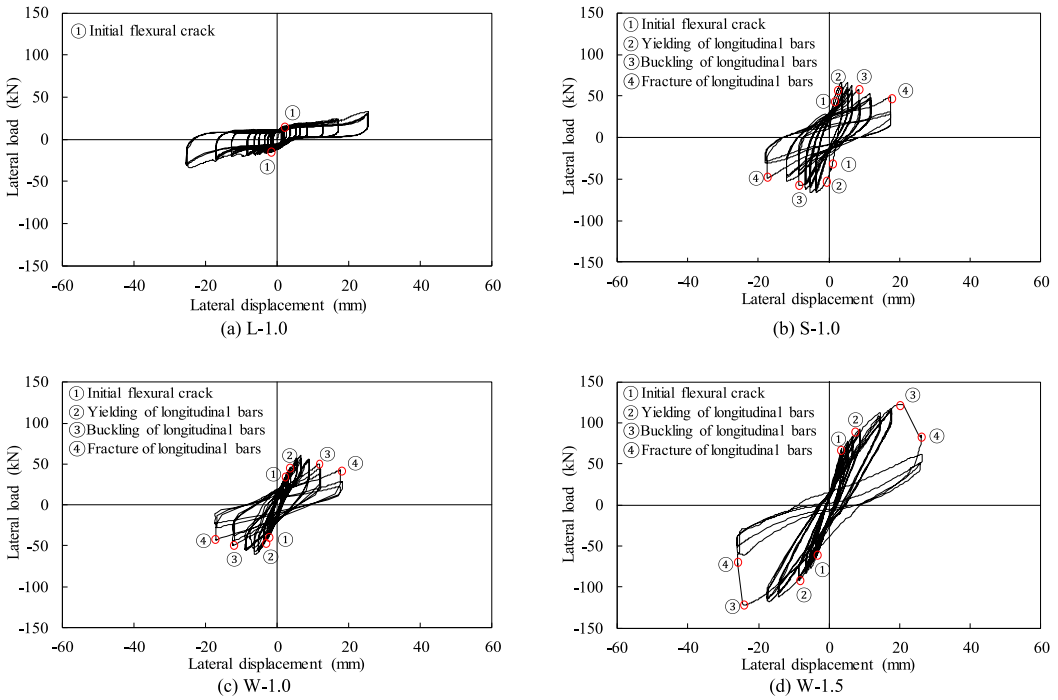

Fig. 6. – Lateral load–displacement relationship of HMI-panel specimens under cyclic in-plane loading.

Table 5
– Summary of experimental results for HMI-panel specimens under cyclic in-plane loading.

Specimens	P_{cr} (kN)	P_y (kN)	P_n (kN)	Δ_y (mm)	Δ_n (mm)	μ_Δ	E_{80} (kN·m)	β_r		
								Experimental values	Predicted values (ACI ITG-5.1)	≥ 0.125
L-1.0	15.5	25.5	37.1	17.1	25.4	1.5	–	–	0.125	NG
S-1.0	48.3	51.1	66.6	1.2	3.5	2.9	2266	0.115	0.125	NG
W-1.0	49.1	50.8	62.4	2.2	6.7	3.0	9908	0.165	0.125	OK
W-1.5	68.1	83.8	122.2	6.5	17.8	2.7	15373	0.175	0.125	OK

Note: P_{cr} = initial cracking load, P_y = yielding load, P_n = peak load, Δ_y = deflection at P_y, Δ_n = deflection at P_n, μ_Δ = displacement ductility ratio, E_{80} = the cumulative dissipated energy value at 80 % of the peak load after the peak load, and β_r = the relative energy dissipation ratio at 80 % of the peak load after the peak load.

specimens connected using the conventional splice-sleeve technique and the splice-sleeve-based bolting technique were 66.4 kN and 62.2 kN, respectively, indicating similar levels. Notably, the P_n value for the specimen connected using the splice-sleeve-based bolting technique was approximately 1.96 times higher when designed with $\rho_v = 1.5\rho_{v(\min)}$ than when designed with $\rho_v = 1.0\rho_{v(\min)}$. Consequently, it can be concluded that when the splice-sleeve-based bolting technique is applied to the HMI-panel specimens and they are adequately reinforced with vertical reinforcements, they can achieve lateral loads (P_{cr} and P_n) comparable to those of the conventional splice-sleeve technique.

4.4. Displacement ductility ratio (μ_Δ)

The displacement ductility ratios (μ_Δ) of the HMI-panel specimens were evaluated using the following equation proposed by Park and Paulay [29].

$$\mu_\Delta = \Delta_n / \Delta_y \tag{1}$$

where Δ_n is the displacement at P_n and Δ_y is the displacement at the yield state of the HMI-panel specimens. The yield state of the HMI-panel specimens was assumed to be the intersection point of a vertical line drawn from the point where the slope was 75 % of the peak load; the horizontal line represents the peak load [19]. As summarized in Table 5, the μ_Δ value of the specimens connected using the L-shaped steel-plate-based bolting technique, which exhibited dominant sliding behavior, was low at 1.5. In contrast, the μ_Δ values of

the specimens connected using the conventional splice-sleeve technique and the splice-sleeve-based bolting technique were in the range of 2.7–3.0, which were on average 1.91 times higher than that of the specimens connected using the L-shaped steel-plate-based bolting technique. Additionally, despite being designed with $\rho_v = 1.5\rho_{v(\min)}$, the μ_Δ value of the specimens connected using the splice-sleeve-based bolting technique was similar to that of conventional reinforced concrete beams (approximately 2.50–2.68). Consequently, it can be concluded that applying the splice-sleeve-based bolting technique to HMI-panel specimens allows for sufficient ductility comparable to that achieved with the conventional splice-sleeve technique.

4.5. Dissipated energy (E_{cd})

Tables 5 and 6, and Fig. 7 show the cumulative dissipated energy (E_{cd}) obtained from the measured lateral load–displacement relationships of the HMI-panel specimens. Dissipation capacity was calculated as the cumulative area enclosed by the hysteresis loops of the lateral load–displacement relationship under cyclic in-plane loading, representing the energy dissipated in each cycle (Fig. 8). The E_{cd} value gradually increased, and after 10 cycles, the rate of increase in E_{cd} value became significantly more pronounced. In particular, the rate of increase was the lowest for the HMI-panel specimen connected using the L-shaped steel-plate-based bolting technique. The E_{cd} value at 80 % of the peak load after the peak load (E_{80}) was not obtained for the HMI-panel specimen connected using the L-shaped steel-plate-based bolting technique because the specimen was terminated after reaching the peak load. Meanwhile, the HMI-panel specimen connected using the splice-sleeve-based bolting technique exhibited a similar rate of increase as that of the specimen connected using the conventional splice-sleeve technique throughout the entire test duration. In particular, the E_{80} value measured in the HMI-panel specimen connected using the splice-sleeve-based bolting technique was 9908 kN mm, approximately 4.37 times higher than the HMI-panel specimen connected using the conventional splice-sleeve technique. Additionally, despite being designed with $\rho_v = 1.5\rho_{v(\min)}$, the E_{80} value of the specimens connected using the splice-sleeve-based bolting technique was 1.55 times higher than that of the specimens using the splice-sleeve-based bolting technique, indicating a value of 15373 kN mm. Consequently, it can be concluded that applying the splice-sleeve-based bolting technique to HMI-panel specimens allows for sufficient dissipated energy, which is more than or equivalent to that achieved with the conventional splice-sleeve technique.

According to ACI ITG-5.1 [30], the dissipated energy at the drift ratio limit is a key indicator for assessing the energy absorption capacity when evaluating the absolute emulation of PC structural walls, particularly intermediate or special shear walls. The drift ratio limit typically denotes the stage at which the energy absorption capacity is assessed, commonly determined based on the post-peak behavior. Accordingly, PC structural walls are required to exhibit a minimum level of dissipated energy, even as this capacity decreases after the peak load. However, since HMI-panels are not classified as structural walls, there are limitations to directly applying the drift ratio limit prescribed by ACI ITG-5.1 [30]. Therefore, the post-peak energy absorption capacity was evaluated at the point corresponding to 80 % of the peak load after the maximum load. The relative energy dissipation ratio (β_r) calculated at this stage was then assessed to determine if it surpasses the required value of 0.125 specified in ACI ITG-5.1 [30] (Table 5). Fig. 9 shows the calculation method of the β_r value. The β_r values of the HMI-panel specimen connected using the L-shaped steel-plate-based bolting technique and the conventional splice-sleeve technique were below 0.125, indicating that these connection techniques are not effective in mitigating the reduction of post-peak energy absorption capacity. However, the β_r values of the HMI-panel specimen connected using connected using the splice-sleeve-based bolting technique were 0.164 and 0.175 for the specimens designed with $\rho_v = 1.0\ \rho_{v(\min)}$ (min) and $\rho_v = 1.5\ \rho_{v(\min)}$, respectively. These values were 1.32 times and 1.4 times higher than the required value of 0.125 specified in ACI ITG-5.1 [30], respectively. Consequently, it can be concluded that the application of the splice-sleeve-based bolting technique to HMI-panel specimens enables sufficient post-peak dissipated energy, exceeding that provided by the conventional splice-sleeve technique.

5. Comparison with predictions

5.1. Cracking flexural moment (M_{cr})

The cracking flexural moment (M_{cr}) of the HMI panel specimen was evaluated using the following equation presented by ACI 318-19 [23]:

Table 6
– Cumulative dissipated energy from hysteresis loops in lateral load–displacement.

Specimens	Cumulative dissipated energy (kN·m)										
	d_r = 0.043 %	d_r = 0.055 %	d_r = 0.07 %	d_r = 0.1 %	d_r = 0.14 %	d_r = 0.2 %	d_r = 0.25 %	d_r = 0.33 %	d_r = 0.5 %	d_r = 0.67 %	d_r = 1.0 %
L-1.0	135	300	526	832	1254	1848	2567	3537	5026	6939	9756
S-1.0	–	–	–	–	802	1932	3386	5196	6664	7913	–
W-1.0	137	276	519	863	1297	1948	2932	4828	7587	10241	–
W-1.5	–	–	–	–	663	1549	2596	4021	7072	10745	15931

Note: d_r = draft ratio.

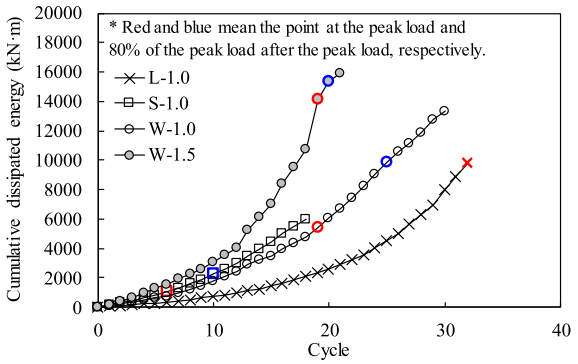

Fig. 7. – Cumulative dissipated energy from hysteresis loops in lateral load–displacement relationships of HMI-panel specimens.

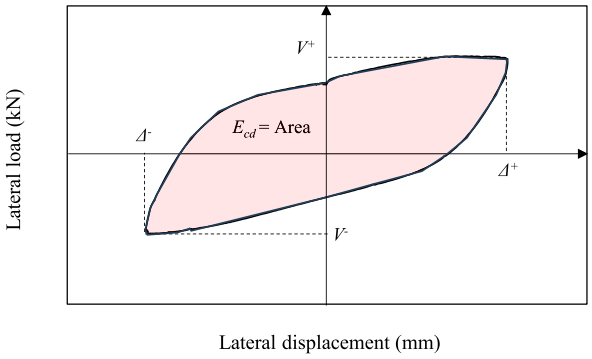

Fig. 8. – Calculation of dissipated energy from hysteresis loops in lateral load–displacement relationships.

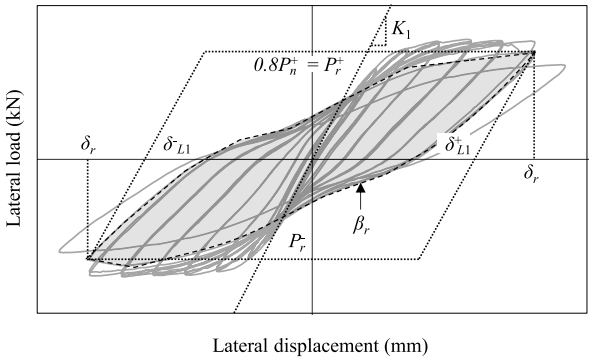

Fig. 9. – Calculation method of the β_r value in lateral load–displacement relationships.

$$M_{cr} = \frac{f_r I_{tr}}{y_t} \tag{2}$$

$$f_r = 0.63\lambda\sqrt{f_c'} \tag{3}$$

where, f_r is the rupture modulus, I_{tr} is the second moment of the transformed area, y_t is the distance from the centroid of the cross-section to the tensile fiber, and λ is the coefficient for lightweight aggregate concrete (normal-weight concrete = 1.0, sand lightweight aggregate concrete = 0.85, and all-lightweight aggregate concrete = 0.75). In this study, all-lightweight aggregate concrete was used to manufacture all the HMI panel specimens. Therefore, 0.75 for λ was applied to Eq. (3). Table 7 summarizes the predicted ($M_{cr(\text{pre.})}$) and experimental ($M_{cr(\text{exp.})}$) values of M_{cr} for HMI panel specimens. The safety of M_{cr} was evaluated by using the ratio of $M_{cr(\text{exp.})}$ to $M_{cr(\text{pre.})}$. A ratio ($M_{cr(\text{exp.})}/M_{cr(\text{pre.})}$) greater than 1.0 indicates that the M_{cr} of the HMI panel specimen sufficiently exceeds the

value predicted by ACI 318-19 [23]. The specimen connected using the L-shaped steel-plate-based bolting technique was overestimated, with an observed $M_{cr(\exp.)}/M_{cr(\text{pre.})}$ value of 0.24. This can be attributed to the significant slip displacements that occurred between the circular steel pipes and the threaded bolts used in the connection, as observed in the Section of 5.1 crack propagation and failure mode. The $M_{cr(\exp.)}/M_{cr(\text{pre.})}$ value of the specimen connected using the conventional splice-sleeve technique and splice-sleeve-based bolting technique was 0.76 and 0.78, respectively, indicating an overestimation. This can be attributed to the low fracture modulus of the bottom ash aggregate-based concrete and the insufficient amount of longitudinal reinforcement. However, the $M_{cr(\exp.)}/M_{cr(\text{pre.})}$ value obtained from the HMI panel specimen designed using $\rho_v = 1.5\rho_{v(\min)}$ was 1.04, indicating an underestimation. Consequently, it can be concluded that the HMI panel specimen can achieve sufficient M_{cr} to be assessed as safe according to ACI 318-19 [23] when splice-sleeve-based bolting technique is applied and vertical reinforcements are designed with $\rho_v = 1.5\rho_{v(\min)}$.

5.2. Maximum flexural moment (M_n)

The maximum flexural moment (M_n) of the HMI-panel specimen was evaluated using the following equation, considering the concept of the equivalent stress block specified in ACI 318-19 [23] and the stress state of the vertical reinforcement (tensile or compressive stress):

$$M_n = 0.85f_c'ab\left(c_u - \frac{a}{2}\right) + |A_{s1}f_{s1}(c_u - d_1)| + |A_{s2}f_{s2}(c_u - d_2)| + \cdots + \left|A_{s6}f_{s6}(c_u - d_6)\right| + \left|A_{s7}f_{s7}(c_u - d_7)\right| \quad (4)$$

where, f_c' is the compressive strength of the concrete, a is the depth of the equivalent stress block, b is the width of the HMI-panel, c_u is the depth of the neutral axis, A_{si} is the cross-sectional area of i-th vertical reinforcement, f_{si} is the stress of i-th vertical reinforcement, and d_i is the depth of i-th vertical reinforcement. In Eq. (4), the c_u value is determined based on the equilibrium of forces and the assumption that the compressive extreme fiber strain at the ultimate state (ε_{cu}) is 0.003. Vertical reinforcements located at depths greater than the c_u ($c_u \le d_i$) were calculated under tensile stress, whereas those at a shallower depth ($c_u > d_i$) were calculated under compressive stress. For example, if c_u is less than d_3, this can be summarized as follows:

$$c_u = \frac{A_{s7}f_{s7} + A_{s6}f_{s6} + \cdots + A_{s3}f_{s3} - A_{s2}f_{s2} - A_{s1}f_{s1}}{0.85f_c'b\beta_1} \quad (5)$$

where, β_1 is the depth coefficient of the concrete equivalent stress block. In Eq. (5), the stress in the vertical reinforcement at position i was assumed to be f_y when the calculated strain exceeded the yield strain (0.0022). The assumed ε_{cu} (0.003) and calculated c_u from the equilibrium of forces for the HMI panel specimen were between 60 and 84 mm, which were smaller than the d_1. Table 6 summarizes the predicted ($M_{n(\text{pre.})}$) and experimental ($M_{n(\exp.)}$) values of M_n for HMI panel specimens. The safety of M_n was evaluated by using the ratio of $M_{n(\exp.)}$ to $M_{n(\text{pre.})}$. A ratio ($M_{n(\exp.)}/M_{n(\text{pre.})}$) greater than 1.0 indicates that the M_n of the HMI panel specimens sufficiently exceeds the value predicted by ACI 318-19 [23]. The $M_{n(\exp.)}/M_{n(\text{pre.})}$ value of the specimen connected using the L-shaped steel-plate-based bolting technique was 0.42, indicating an overestimation. This can be attributed to the significant slip displacements that occurred between the circular steel pipes and the threaded bolts used in the connection, which led to insufficient transfer of lateral loads. The specimens connected using the conventional splice-sleeve technique and splice-sleeve-based bolting technique were underestimated, with an observed $M_{n(\exp.)}/M_{n(\text{pre.})}$ value of 1.09. However, the underestimation was not significantly high and remained below 9 %. Notably, the $M_{n(\exp.)}/M_{n(\text{pre.})}$ obtained from the HMI panel specimen designed with $\rho_v = 1.5\rho_{v(\min)}$ was 1.06, indicating an underestimation. The reason why the ratios of $M_{n(\exp.)}/M_{n(\text{pre.})}$ were within the range of 1.02–1.09 is that the tensile strength increases as the outermost longitudinal reinforcement reaches the hardening region. Consequently, it can be concluded that the HMI panel specimen can achieve sufficient M_n to be assessed as safe according to ACI 318-19 [23] when the splice-sleeve-based bolting technique is applied and vertical reinforcements are designed with $\rho_v = 1.5\rho_{v(\min)}$.

5.3. Displacement ductility ratio (μ_Δ)

The μ_Δ of the HMI panel specimen was evaluated by comparing the analytical values obtained from the lateral load–displacement relationship predicted by the one-dimensional nonlinear analysis (1-DNA) procedure established by Mun et al. [24] with the experimental results. Fig. 10 presents the flowchart of the one-DNA procedure for panels integrated with a base without a base-to-panel joint. The established one-DNA procedure can be summarized as follows: 1) The compressive fiber strain (ε_c) is incremented from 0.0000 to 0.0300 at the critical section. 2) For each incremented ε_c, the depth of the neutral axis (c_i) is assumed. 3) The strains of each material are determined based on the assumed c_i. 4) The stresses are calculated from the stress–strain relationships of each material, and the compressive and tensile forces are computed from the areas of each infinitesimal element. 5) The compressive and tensile forces are summed to verify whether the equilibrium of forces is satisfied. 6) If the equilibrium condition is not satisfied, return to step 2) and re-assume c_i. This procedure is repeated until the equilibrium condition is satisfied. 7) Based on the determined c_i, curvature and flexural moment are calculated. 8) The lateral load is determined from the calculated flexural moment, and displacement is estimated using the concept of an idealized curvature distribution and equivalent plastic hinge length (l_p). 9) The lateral load–displacement curve for each increment of ε_c is derived, from which μ_Δ is determined. The following equation proposed by Yang et al. [31] was used as the constitutive equation for the compressive concrete in procedure 4):

Table 7
– Experimental and predicted flexural moments of the HMI-panel specimens under cyclic in-plane loading.

Specimens	Experiments			Predictions			Comparison		
	M_{cr} (kN·m) (1)	M_n (kN·m) (2)	μ_Δ (3)	$M_{cr(\text{pre.})}$ (kN·m) (4)	$M_{n(\text{pre.})}$ (kN·m) (5)	$\mu_{\Delta(\text{pre.})}$ (6)	(1)/(4)	(2)/(5)	(3)/(6)
L-1.0	40.8	97.6	1.5	167.5	232.1	2.5	0.24	0.42	0.61
S-1.0	127.0	175.2	2.9	166.6	160.9	2.6	0.76	1.09	1.12
W-1.0	129.1	164.1	3.0	166.6	161.6	2.6	0.78	1.02	1.13
W-1.5	179.1	321.4	2.7	173.0	302.2	2.4	1.04	1.06	1.15

Note: M_{cr} = cracking flexural moment, M_n = maximum flexural moment, μ_Δ = displacement ductility ratio, $M_{cr(\text{pre.})}$ and $M_{n(\text{pre.})}$ = cracking and maximum flexural moment by ACI 318-19, respectively, and $\mu_{\Delta(\text{pre.})}$ = displacement ductility ratio by predicted by Yang et al.

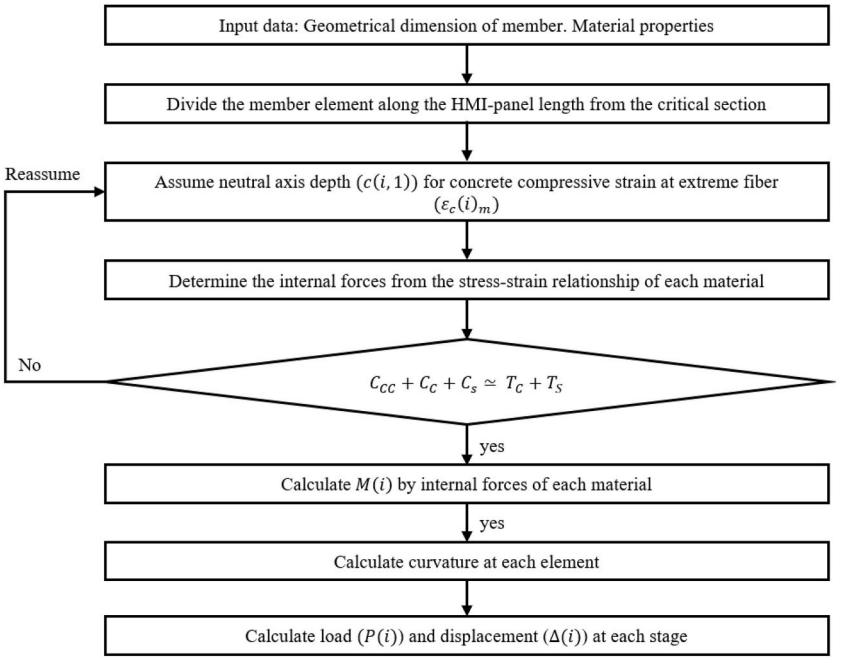

Fig. 10. – Flow chart of one-DNA procedure.

$$\mathrm{f}_c = \left\{ \frac{(\beta+1)(\varepsilon_c/\varepsilon_0)}{(\varepsilon_c/\varepsilon_0)^{\beta+1}+\beta} \right\} f_c' \tag{6}$$

$$\beta = \begin{cases} 0.20\exp(0.73\zeta) & \text{for } \varepsilon_c \le \varepsilon_0 \\ 0.41\exp(0.77\zeta) & \text{for } \varepsilon_c > \varepsilon_0 \end{cases} \tag{7}$$

$$\varepsilon_0 = 0.0016\mathrm{Exp}\{240(f_c'/E_c)\} \tag{8}$$

where, f_c is the concrete compressive stress corresponding to the strain, β is a factor that accounts for the slopes of the ascending and descending branches of the stress–strain curve, ε_c is the variable compressive strain, ε_0 is the strain at the peak stress of the concrete, and E_c is the modulus of elasticity of the concrete. Additionally, the following equation proposed by Mattock [32] was used for l_p in Procedure 8):

$$\mathrm{l}_p = 0.5d + 0.05z \tag{9}$$

where, d is the effective depth and z is the distance from the critical section to the inflection point. As shown in Table 6, the safety of μ_Δ was evaluated based on the ratio of the experimental ($\mu_{\Delta(\text{exp.})}$) to predicted ($\mu_{\Delta(\text{pre.})}$) values. A value greater than 1.0 indicates that the μ_Δ of the HMI panel specimen is higher than the value predicted by one-DNA. The $\mu_{\Delta(\text{exp.})}/\mu_{\Delta(\text{pre.})}$ of the specimens connected using the L-shaped steel-plate-based bolting technique was 0.61, indicating an overestimation. In contrast, the $\mu_{\Delta(\text{exp.})}/\mu_{\Delta(\text{pre.})}$ of specimens connected using the conventional splice-sleeve technique and splice-sleeve-based bolting technique ranged from 1.12 to 1.15,

indicating underestimation. These values were, on average, 1.87 times higher than those of specimens connected using the L-shaped steel-plate-based bolting technique. Consequently, it can be concluded that when applying the splice-sleeve-based bolting technique, the HMI panel specimen can achieve a sufficient μ_{Δ}, comparable to that of panels integrated with a base without a base-to-panel joint.

6. Flexural design procedure for HMI-penels connected with the splice-sleeve-based bolting technique

Based on the results presented above, the flexural design procedure for HMI-panels with the splice-sleeve-based bolting technique can be summarized as follows: 1) The design loads corresponding to axial force, shear, and flexural moment acting on HMI-panels are evaluated. 2) Based on these design loads, the cross-sectional dimensions and material properties of the HMI-panels are specified. The compressive strength of lightweight aggregate concrete is taken as an average of 24 MPa and the average unit weight of concrete (ρ_c) is assumed to be 1500 kg/m^3. The vertical reinforcement ratio is provided at not less than 1.5 $\rho_{s(\min)}$ and the horizontal reinforcement ratio is determined to adequately resist the applied shear forces. 3) The connection between the HMI-panels and the base employs the splice-sleeve-based bolting technique, in which the sleeves inserted into the panels are confined by closed horizontal reinforcement. The sleeve details are defined in accordance with fib 2010 [33], and the mortar placed inside the sleeve must achieve a compressive strength of at least 80 MPa to prevent reinforcement pullout or failure until the stress in the vertical reinforcement reaches 1.25 times their yield strength. 4) Finally, the flexural moment capacity of the HMI-panels is verified using Eqs. (4) and (5), and if it the design is found to be inadequate, the amount of vertical reinforcement is increased and the procedure is repeated. Through this iterative process, HMI-panels designed with the splice-sleeve-based bolting technique can ensured to provide both sufficient flexural moment capacity and enhanced post-peak energy absorption capacity.

7. Conclusions

Cyclic lateral load tests were conducted to evaluate the seismic in-plane performance of meta-based insulated precast lightweight aggregate concrete panels (HMI-panels) using a newly developed splice-sleeve-based bolting technique. The following conclusions were drawn.

1. The L-shaped steel-plate-based bolt technique proved ineffective in transferring lateral forces owing to crack concentration and significant sliding displacement at the base-to-panel joint. It exhibited typical sliding behavior, with 68 % and 44 % lower lateral resistance capacities (P_{cr} and P_n, respectively) and a 48 % lower displacement ductility ratio (μ_{Δ}) than HMI panels with the conventional splice-sleeve technique.
2. The splice-sleeve-based bolt technique demonstrated superior lateral force transfer capacity and ductility, performing equally to or better than the conventional splice-sleeve technique in terms of flexural behavior. Notably, the P_{cr} and P_n of HMI panels with the splice-based bolt technique were 3.17 times and 1.68 times higher, respectively, than those with L-shaped steel-plate-based bolt technique, indicating significantly enhanced flexural resistance.
3. When the vertical reinforcement ratio was increased by 1.5 times in the HMI panels using the splice-sleeve-based bolt technique, they maintained a similar level of E_{80} while achieving a 6.78 times higher lateral load resistance compared to HMI panels using the conventional splice-sleeve technique.
4. A comparison of the experimental results with predictions based on the ACI 318-19 standards verified that the splice sleeve-based bolt technique ensures structural safety at cracking and maximum strength moments when the vertical reinforcement ratio is increased by a factor of 1.5.
5. The splice-sleeve-based bolt technique is considered to be an effective approach for improving the seismic performance of HMI panels. However, the HMI panel proposed in this study was primarily designed for application as external cladding and is optimized for use as a non-load-bearing wall. Accordingly, its main loading conditions are limited to relatively low loads, such as self-weight and wind loads, and its applicability to load-bearing walls or moderate to high load conditions is restricted. In addition, the effectiveness of the panel has been verified within the dimensional range used in the experiments (350 mm × 1200 mm × 2775 mm); applications outside of this range, including different shapes or thicknesses, require further validation. The materials employed are also limited to those specified in this study (e.g., bottom ash aggregate concrete), and the applicability to other materials would necessitate separate experimental verification.

CRediT authorship contribution statement

Keun-Hyeok Yang: Writing – review & editing, Resources, Project administration, Methodology, Investigation, Formal analysis, Data curation. **Ju-Hyun Mun:** Writing – review & editing, Writing – original draft, Supervision, Methodology, Funding acquisition, Formal analysis, Conceptualization. **Jong-Won Kim:** Writing – review & editing, Writing – original draft, Validation, Investigation, Formal analysis, Data curation. **Hye-Ji Lee:** Writing – review & editing, Investigation, Formal analysis, Data curation.

Declaration of competing interest

The author declare that they have no known competing financial interests or personal relationships that could have appeared to influence the work reported in this paper.

Acknowledgments

This work was supported by the National Research Foundation of Korea (NRF) grant funded by the Korea Government (MSIT) (No. RS-2024-00459490, RS-2024-00405537 and RS-2025-00561383).

Data availability

No data was used for the research described in the article.

References

[1] Y. Choi, E.S. Jeong, J.H. Mun, K.H. Yang, S.J. Lee, Thermal performance and condensation analysis of insulated concrete panels using a thermal-meta structure, Appl. Therm. Eng. 230 (2023) 120761, https://doi.org/10.1016/j.applthermaleng.2023.120761.
[2] W. Qiao, X. Yin, H. Zhang, D. Wang, Experimental study of insulated sandwich concrete wall connections under cyclic loading, Structures 28 (2020) 2000–2012, https://doi.org/10.1016/j.istruc.2020.10.029.
[3] A. Memari, N. Simmons, R. Sonlonsky, Unitized curtain wall systems joint performance with re-entrant corners under seismic racking testing, J. Build. Eng. 40 (2021) 102715, https://doi.org/10.1016/j.jobe.2021.102715.
[4] O.M. Kaylrga, F. Altun, Investigation of earthquake behavior of unreinforced masonry buildings having different opening sizes: experimental studies and numerical simulation, J. Build. Eng. 40 (2021) 102666, https://doi.org/10.1016/j.jobe.2021.102666.
[5] C. Zhang, B. Ling, W. Huang, X. Deng, C. Ding, J. Gao, S. Zhang, Cyclic behavior of semi-rigid steel frame infilled with damping wall panels, J. Build. Eng. 51 (2022) 104238, https://doi.org/10.1016/j.jobe.2022.104238.
[6] Q. Yu, J. Wu, X. Gu, L. Wang, Seismic behavior of hinged steel frames with masonry infill walls, J. Build. Eng. 77 (2023) 107536, https://doi.org/10.1016/j.jobe.2023.107536.
[7] Q. Fang, J. Sun, H. Qiu, H. Jiang, B.D. Lago, F. Biondini, Experimental evaluation on the seismic behavior of precast concrete shear walls with slip-friction devices, J. Build. Eng. 52 (2022) 104507, https://doi.org/10.1016/j.jobe.2022.104507.
[8] Y. Ye, Z. Hou, P. Qiao, Z. Wang, Q. Kang, Experimental study on seismic behavior of a new fully precast rocking beam-column joint, J. Build. Eng. 62 (2022) 105337, https://doi.org/10.1016/j.jobe.2022.105337.
[9] Y.C. Zhong, F. Xiong, M.M. Ran, J. Chen, Q. Ge, Y. Lu, " Seismic behavior of a novel bolt-connected horizontal joint for precast RC wall panel structures: experimental and numerical analysis", J. Build. Eng. 52 (2022) 104451 https://doi.org/10.1016/j.jobe.2022.104451.
[10] M. Khanmohammadi, M. Eshraghi, S. Sayadi, M.G. Mashhadinezhad, Post-earthquake seismic assessment of residential buildings following Sarpol-e zahab (Iran) earthquake (Mw7.3) part 1: damage types and damage states, Soil Dynam. Earthq. Eng. 173 (2023) 108121, https://doi.org/10.1016/j.soildyn.2023.108121.
[11] KDS, Standard for Seismic Design of Buildings (KDS 41 17 00: 2022), Korean Design Standard, Goyang–si, Korea, 2022.
[12] Q. Deng, Q. Gu, Y. Tan, B. Peng, Y. Zhang, X. Wang, Experimental analysis on the out-of-plane structural performance of single-face superposed shear walls with different horizontal connections, J. Build. Eng. 75 (2023) 107010, https://doi.org/10.1016/j.jobe.2023.107010.
[13] K.H. Yang, J.H. Mun, Y.B. Jung, J.W. Kim, S.J. Lee, Y.J. Choi, Flexural behaviour of precast lightweight aggregate concrete insulation panels, J. Build. Eng. 74 (2023) 106861, https://doi.org/10.1016/j.jobe.2023.106861.
[14] R. O'Hegarty, O. Kinnane, Review of precast concrete sandwich panels and their innovations, Constr. Build. Mater. 233 (2020) 117145, https://doi.org/10.1016/j.conbuildmat.2019.117145.
[15] A. Elbelbisi, A. El-Sisi, L. Elgholmy, Z. Helal, H. Elemam, A. Saucier, H. Salim, Experimental study on non-load bearing multi-span sandwich wall panels for blast mitigation, J. Build. Eng. 98 (2024) 110968, https://doi.org/10.1016/j.jobe.2024.110968.
[16] H. Hou, W. Wang, B. Qu, C. Dai, Testing of insulated sandwich panels with GFRP shear connectors, Eng. Struct. 209 (2020) 109954.
[17] K.B. Choi, W.C. Choi, L. Feo, S.J. Jang, D.Y. Yun, In-plane shear behavior of insulated precast concrete sandwich panels reinforced with corrugated GFRP shear connectors, Compos. B Eng. 79 (2015) 419–429, https://doi.org/10.1016/j.compositesb.2015.04.056.
[18] P. Seifi, R.S. Henry, J.M. Ingham, In-plane cyclic testing of precast concrete wall panels with grouted metal duct base connections, Eng. Struct. 184 (2019) 85–98, https://doi.org/10.1016/j.engstruct.2019.01.079.
[19] H. Zhang, W. Huang, C. Han, Q. Li, L. Ge, Test and analysis on in-plane shear behavior of precast concrete hollow core slabs, Structures 56 (2023) 104988, https://doi.org/10.1016/j.istruc.2023.104988.
[20] H. Tawil, C.G. Tan, N.H. Ramli Sulong, F.M. Nazri, M.F. Shamsudin, N.M. Bunnori, Optimization of shear resistance in precast concrete sandwich wall panels using an S-type shear connector, Buildings 14 (6) (2024) 1725, https://doi.org/10.3390/buildings14061725.
[21] S.M. Kang, J.H. Kang, H.J. Son, S.I. Kim, T.S. Eom, H.J. Hwang, D.J. Kim, In-plane seismic performance of precast concrete hollow-core slab panels for basement walls, Structures 63 (2024) 106478, https://doi.org/10.1016/j.istruc.2024.106478.
[22] H. Yu, H. Zhang, P. Zhang, K. Ma, H. Zhang, J. Qiao, Research on seismic behavior of precast concrete shear wall with new steel plate-bolted horizontal connection, J. Build. Eng. 85 (2024) 108719, https://doi.org/10.1016/j.jobe.2024.108719.
[23] ACI Committee 318, Building Code Requirements for Structural Concrete (ACI 318-19) and Commentary, American Concrete Institute, Farmington Hills, MI, 2019.
[24] J.H. Mun, K.H. Yang, Y. Lee, Seismic tests on heavyweight concrete shear walls with wire ropes as lateral reinforcement, ACI Struct. J. 113 (4) (2016) 664–675, https://doi.org/10.14359/51688615.
[25] J.H. Sim, J.W. Kim, K.H. Yang, Optimum details of thermal-meta structures for enhancing the isulation capacity of concrete panels, J. Arch. Inst. Kor. 38 (5) (2022) 243–250, https://doi.org/10.5659/JAIK.2022.38.5.243.
[26] J.W. Kim, K.H. Yang, J.H. Mun, Evaluation of shear friction performance at construction joints of lightweight concrete using bottom ash aggregates and air foams, J. Arch. Inst. Kor. 36 (9) (2020) 139–144, https://doi.org/10.5659/JAIK.2020.36.9.139.
[27] Korea Agency for Technology and Standards (KATS), Aggregates for Concrete (KS F 2527). Korea Standard Association (KSA), 2022. Seoul, Korea.
[28] FEMA 356, Prestandard and Commentary for the Seismic Rehabilitation of Buildings (FEMA 356), Applied Technology Council (ATC), Washington, DC, 2000.
[29] R. Park, T. Paulay, Reinforced Concrete Structures, John Wiley and Sons, New York, 1975.
[30] ACI ITG-5.1-07, Acceptance Criteria for Special Unbonded Post-tensioned Precast Structural Walls Based on Validation Testing, American Concrete Institute, Farmington Hills, MI, 2008, 2008.
[31] K.H. Yang, J.H. Mun, M.S. Cho, T.H.K. Kang, Stress-strain model for various unconfined concretes in compression, ACI Struct. J. 111 (4) (2014) 819–826, https://doi.org/10.14359/51686631.
[32] A.H. Mattock, Discussion of rotational capacity of reinforced concrete beams by W. G. Corley, J. Struct. Div. 93 (1967) 519–522.
[33] Fib (CEB-FIP), Structural Concrete: Textbook on Behavior, Design and Performance, International federation for structural concrete, Lausanne, Switzerland, 2010.